

Nucleon resonances in ω photoproduction

Yongseok Oh,^{a*} Alexander I. Titov,^{b†} and T.-S. H. Lee^{c‡}

^a *Institute of Physics, Academia Sinica, Nankang, Taipei 11529, Taiwan*

^b *Bogoliubov Laboratory of Theoretical Physics, JINR, Dubna 141980, Russia*

^c *Physics Division, Argonne National Laboratory, Argonne, Illinois 60439*

Abstract

The role of the nucleon resonances (N^*) in ω photoproduction is investigated by using the resonance parameters predicted by Capstick and Roberts [Phys. Rev. D **46**, 2864 (1992); **49**, 4570 (1994)]. In contrast with the previous investigations based on the $SU(6) \times O(3)$ limit of the constituent quark model, the employed $N^* \rightarrow \gamma N$ and $N^* \rightarrow \omega N$ amplitudes include the configuration mixing effects due to the residual quark-quark interactions. The contributions from the nucleon resonances are found to be significant relative to the non-resonant amplitudes in changing the differential cross sections at large scattering angles and various spin observables. In particular, we suggest that a crucial test of our predictions can be made by measuring the parity asymmetry and beam-target double asymmetry at forward scattering angles. The dominant contributions are found to be from $N_{\frac{3}{2}}^+(1910)$, a missing resonance, and $N_{\frac{3}{2}}^-(1960)$ which is identified as the $D_{13}(2080)$ of the Particle Data Group.

PACS number(s): 13.88.+e, 13.60.Le, 14.20.Gk, 25.20.Lj

Typeset using REVTeX

*E-mail address: yoh@phya.yonsei.ac.kr, Address after Aug. 1, 2000: Institute of Physics and Applied Physics, Yonsei University, Seoul 120-749, Korea

†E-mail address: atitov@thsun1.jinr.ru

‡E-mail address: lee@anlphy.phy.anl.gov

I. INTRODUCTION

The constituent quark models predict a much richer nucleon excitation spectrum than what have been observed in pion-nucleon scattering [1]. This has been attributed to the possibility that a lot of the predicted nucleon resonances (N^*) could couple weakly to the πN channel. Therefore it is necessary to search for the nucleon excitations in other reactions to resolve the so-called “missing resonance problem.” Electromagnetic production of vector mesons (ω, ρ, ϕ) is one of such reactions and is being investigated experimentally, e.g., at Thomas Jefferson National Accelerator Facility, ELSA-SAPHIR of Bonn, GRAAL of Grenoble, and LEPS of SPring-8.

The role of the nucleon excitations in vector meson photoproduction was studied recently by Zhao *et al.* [2–4] using an effective Lagrangian method within the $SU(6) \times O(3)$ constituent quark model. With the meson-quark coupling parameters adjusted to fit the existing data, they found that the single polarization observables are sensitive to the nucleon resonances.

We are motivated by the predictions by Capstick and Roberts [5,6]. They started with a constituent quark model which accounts for the configuration mixing due to the residual quark-quark interactions [7]. The predicted baryon wave functions are considerably different from those of the $SU(6) \times O(3)$ model employed by Zhao *et al.* in Refs. [2–4]. The second feature of the predictions from Refs. [5,6] is that the meson decays are calculated from the correlated wave functions by using the 3P_0 model [8]. Thus it would be interesting to see how these predictions differ from those of Refs. [2–4] and can be tested against the data of vector meson photoproduction.

We will focus on ω photoproduction in this work, simply because its non-resonant reaction mechanisms are much better understood. It was fairly well established [9–13] already during the years around 1970 that this reaction is dominated by diffractive processes at high energies and by one-pion exchange at low energies. The diffractive part can be described by the Pomeron exchange model. The calculation of the one-pion exchange amplitude has been recently revived by Friman and Soyeur [14]. It is therefore reasonable to follow the earlier theoretical analyses [11] and assume that the non-resonant amplitude of ω photoproduction can be calculated from these two well-established mechanisms with some refinements. The resulting model then can be a starting point for investigating the N^* effects. This approach is similar to the previous investigation by Zhao *et al.* [2,3].

In Sec. II, we give explicit expressions for the non-resonant amplitudes employed in our calculations. The calculations of resonant amplitudes from Refs. [5,6] are detailed in Sec. III and the results are presented in Sec. IV. Section V is devoted to discussing possible future developments.

II. NON-RESONANT AMPLITUDES

We assume that the non-resonant amplitude is due to the Pomeron exchange [Fig. 1(a)], pseudoscalar-meson exchange [Fig. 1(b)], and the direct and crossed nucleon terms [Figs. 1(c) and 1(d)]. The four-momenta of the incoming photon, outgoing ω , initial nucleon, and final nucleon are denoted as k , q , p , and p' respectively, which defines $t = (p - p')^2 = (q - k)^2$, $s \equiv W^2 = (p + k)^2$, and the ω production angle θ by $\cos \theta \equiv \mathbf{k} \cdot \mathbf{q} / |\mathbf{k}| |\mathbf{q}|$.

We choose the convention [15] that the scattering amplitude T is related to the S -matrix by

$$S_{fi} = \delta_{fi} - i(2\pi)^4 \delta^4(k + p - q - p') T_{fi} \quad (1)$$

with

$$T_{fi} = \frac{1}{(2\pi)^6} \frac{1}{\sqrt{2E_\omega(\mathbf{q})}} \sqrt{\frac{M_N}{E_N(\mathbf{p}')}} I_{fi} \frac{1}{\sqrt{2|\mathbf{k}|}} \sqrt{\frac{M_N}{E_N(\mathbf{p})}}, \quad (2)$$

where $E_\alpha(\mathbf{p}) = \sqrt{M_\alpha^2 + \mathbf{p}^2}$ with M_α denoting the mass of the particle α . The invariant amplitude can be written as

$$I_{fi} = I_{fi}^{bg} + I_{fi}^{N*}, \quad (3)$$

where the nonresonant (background) amplitude is

$$I_{fi}^{bg} = I_{fi}^P + I_{fi}^{ps} + I_{fi}^N \quad (4)$$

with I_{fi}^P , I_{fi}^{ps} , and I_{fi}^N denoting the amplitudes due to the Pomeron exchange, pseudoscalar-meson exchange, and direct and crossed nucleon terms, respectively. The nucleon excitation term I_{fi}^{N*} will be given in Sec. III.

For the Pomeron exchange, which governs the total cross sections and differential cross sections at low $|t|$ in the high energy region, we follow the Donnachie-Landshoff model [16], which gives [17,18]

$$I_{fi}^P = iM_0(s, t) \bar{u}_{m_f}(p') \varepsilon_\mu^*(\omega) \{k g^{\mu\nu} - k^\mu \gamma^\nu\} \varepsilon_\nu(\gamma) u_{m_i}(p), \quad (5)$$

where $\varepsilon_\mu(\omega)$ and $\varepsilon_\nu(\gamma)$ are the polarization vectors of the ω meson and photon, respectively, and $u_m(p)$ is the Dirac spinor of the nucleon with momentum p and spin projection m . The Pomeron exchange is described by the following Regge parameterization

$$M_0(s, t) = C_V F_1(t) F_V(t) \left(\frac{s}{s_0}\right)^{\alpha_P(t)-1} \exp\left\{-\frac{i\pi}{2}[\alpha_P(t) - 1]\right\}, \quad (6)$$

where $F_1(t)$ is the isoscalar electromagnetic form factor of the nucleon and $F_V(t)$ is the form factor for the vector-meson-photon-Pomeron coupling. We also follow Ref. [16] to write

$$F_1(t) = \frac{4M_N^2 - 2.8t}{(4M_N^2 - t)(1 - t/t_0)^2},$$

$$F_V(t) = \frac{1}{1 - t/M_V^2} \frac{2\mu_0^2}{2\mu_0^2 + M_V^2 - t}, \quad (7)$$

where $t_0 = 0.7 \text{ GeV}^2$. The Pomeron trajectory is known to be $\alpha_P(t) = 1.08 + 0.25t$. (See also Ref. [19]) The strength factor C_V reads $C_V = 12\sqrt{4\pi\alpha_{\text{em}}}\beta_0^2/f_V$ with the vector meson decay constant f_V ($= 17.05$ for the ω meson) and $\alpha_{\text{em}} = e^2/4\pi$. By fitting all of the total cross

section data for ω , ρ , and ϕ photoproduction at high energies, the remaining parameters of the model are determined: $\mu_0^2 = 1.1 \text{ GeV}^2$, $\beta_0 = 2.05 \text{ GeV}^{-1}$, and $s_0 = 4 \text{ GeV}^2$.

The pseudoscalar-meson exchange amplitude can be calculated from the following effective Lagrangians,

$$\begin{aligned}\mathcal{L}_{\omega\gamma\varphi} &= \frac{eg_{\omega\gamma\varphi}}{M_V} \epsilon^{\mu\nu\alpha\beta} \partial_\mu \omega_\nu \partial_\alpha A_\beta \varphi, \\ \mathcal{L}_{\varphi NN} &= -ig_{\pi NN} \bar{N} \gamma_5 \tau_3 N \pi^0 - ig_{\eta NN} \bar{N} \gamma_5 N \eta,\end{aligned}\quad (8)$$

where $\varphi = (\pi^0, \eta)$ and A_β is the photon field. The resulting invariant amplitude is

$$I_{fi}^{ps} = - \sum_{\varphi=\pi,\eta} \frac{iF_{\varphi NN}(t)F_{\omega\gamma\varphi}(t)}{t - M_\varphi^2} \frac{eg_{\omega\gamma\varphi}g_{\varphi NN}}{M_V} \bar{u}_{m_f}(p') \gamma_5 u_{m_i}(p) \epsilon^{\mu\nu\alpha\beta} q_\mu k_\alpha \epsilon_\nu^*(\omega) \epsilon_\beta(\gamma). \quad (9)$$

In the above, we have followed Ref. [14] to include the following form factors to dress the φNN and $\omega\gamma\varphi$ vertices,

$$F_{\varphi NN}(t) = \frac{\Lambda_\varphi^2 - M_\varphi^2}{\Lambda_\varphi^2 - t}, \quad F_{\omega\gamma\varphi}(t) = \frac{\Lambda_{\omega\gamma\varphi}^2 - M_\varphi^2}{\Lambda_{\omega\gamma\varphi}^2 - t}. \quad (10)$$

We use $g_{\pi NN}^2/4\pi = 14$ for the πNN coupling constant. The ηNN coupling constant is not well determined [20]. Here we use $g_{\eta NN}^2/4\pi = 0.99$ which is obtained from making use of the SU(3) symmetry relation [21] together with a recent value of $F/D = 0.575$ [22]. The coupling constants $g_{\omega\gamma\varphi}$ can be estimated through the decay widths of $\omega \rightarrow \gamma\pi$ and $\omega \rightarrow \gamma\eta$ [23] which lead to $g_{\omega\gamma\pi} = 1.823$ and $g_{\omega\gamma\eta} = 0.416$. The cutoff parameters Λ_φ and $\Lambda_{\omega\gamma\varphi}$ in Eq. (10) will be specified in Sec. IV.

We evaluate the direct and crossed nucleon amplitudes shown in Fig. 1(c) and 1(d) from the following interaction Lagrangians,

$$\begin{aligned}\mathcal{L}_{\gamma NN} &= -e\bar{N} \left(\gamma_\mu \frac{1 + \tau_3}{2} A^\mu - \frac{\kappa_N}{2M_N} \sigma^{\mu\nu} \partial_\nu A_\mu \right) N, \\ \mathcal{L}_{\omega NN} &= -g_{\omega NN} \bar{N} \left(\gamma_\mu \omega^\mu - \frac{\kappa_\omega}{2M_N} \sigma^{\mu\nu} \partial_\nu \omega_\mu \right) N,\end{aligned}\quad (11)$$

with the anomalous magnetic moment of the nucleon $\kappa_{p(n)} = 1.79$ (-1.91). There are some uncertainties in choosing the ωNN coupling constants. In this work, we consider $g_{\omega NN} = 7.0 \sim 11.0$ and $\kappa_\omega \approx 0$, which are determined in a study of πN scattering and pion photoproduction [24]. The resulting invariant amplitude reads

$$I_{fi}^N = \bar{u}_{m_f}(p') \epsilon^{\mu*}(\omega) M_{\mu\nu} \epsilon^\nu(\gamma) u_{m_i}(p), \quad (12)$$

where

$$M_{\mu\nu} = -eg_{\omega NN} \left[\Gamma_\mu^\omega(q) \frac{\not{p} + \not{k} + M_N}{s - M_N^2} \Gamma_\nu^\gamma(k) F_N(s) + \Gamma_\nu^\gamma(k) \frac{\not{p} - \not{q} + M_N}{u - M_N^2} \Gamma_\mu^\omega(q) F_N(u) \right] \quad (13)$$

with

$$\Gamma_\mu^\omega(q) = \gamma_\mu - i\frac{\kappa_\omega}{2M_N}\sigma_{\mu\alpha}q^\alpha, \quad \Gamma_\nu^\gamma(k) = \gamma_\nu + i\frac{\kappa_p}{2M_N}\sigma_{\nu\beta}k^\beta, \quad (14)$$

and $s = (p+k)^2$, $u = (p-q)^2$. Here we have followed Ref. [25] to include a form factor

$$F_N(r) = \frac{\Lambda_N^4}{\Lambda_N^4 - (r - M_N^2)^2} \quad (15)$$

with $r = s$ or t . The cutoff parameter Λ_N will be specified later in Sec. IV.

The amplitude (13) is not gauge-invariant because of the form factors $F_N(s)$ and $F_N(u)$. (Note that the terminology ‘‘gauge invariance’’ here only means the ‘‘current conservation’’ conditions $M_{\mu\nu}k^\nu = q^\mu M_{\mu\nu} = 0$ as considered in most investigations.) To restore the gauge invariance, we follow Ref. [26] and modify the amplitude $M_{\mu\nu}$ by using the projection operator $P_{\mu\nu} = g_{\mu\nu} - k_\mu q_\nu / k \cdot q$;

$$M_{\mu\nu} \rightarrow P_{\mu\mu'} M^{\mu'\nu'} P_{\nu'\nu}, \quad (16)$$

which leads to the following modifications in evaluating the amplitude (13):

$$\begin{aligned} \Gamma_\mu^\omega(q) &\rightarrow \Gamma_\mu^\omega(q) - \frac{1}{k \cdot q} k_\mu q \cdot \Gamma^\omega(q), \\ \Gamma_\nu^\gamma(k) &\rightarrow \Gamma_\nu^\gamma(k) - \frac{1}{k \cdot q} q_\nu k \cdot \Gamma^\gamma(k). \end{aligned} \quad (17)$$

The above prescription is certainly very phenomenological, while it is similar to other accepted approaches in literature. Perhaps a more rigorous approach can be developed by extending the work for pseudoscalar meson production [25] to the present case of vector meson production. This is however beyond the scope of this investigation. For our present exploratory purposes, the prescription defined by Eqs. (16) and (17) is sufficient.

III. RESONANT AMPLITUDE

In order to estimate the nucleon resonance contributions we make use of the quark model predictions on the resonance photo-excitation $\gamma N \rightarrow N^*$ and the resonance decay $N^* \rightarrow \omega N$ reported in Refs. [5,6] using a relativised quark model. The resonant amplitude is illustrated in Fig. 1(e). The crossed N^* amplitude, similar to Fig. 1(d), cannot be calculated from the informations available in Refs. [5,6] and are not considered in this work. Here we follow Ref. [24] and write the resonant amplitude in the center of mass frame as [in the convention defined by Eqs. (1) and (2)]

$$I_{m_f, m_\omega, m_i, \lambda_\gamma}^{N^*}(\mathbf{q}, \mathbf{k}) = \sum_{J, M_J} \frac{\mathcal{M}_{N^* \rightarrow N'\omega}(\mathbf{q}; m_f, m_\omega; J, M_J) \mathcal{M}_{\gamma N \rightarrow N^*}(\mathbf{k}; m_i, \lambda_\gamma; J, M_J)}{\sqrt{s} - M_R^J + \frac{i}{2}\Gamma^J(s)}, \quad (18)$$

where M_R^J is the mass of a N^* with spin quantum numbers (J, M_J) , and m_i , m_f , λ_γ , and m_ω are the spin projections of the initial nucleon, final nucleon, incoming photon, and outgoing ω meson, respectively. Here we neglect the effect due to the nonresonant mechanisms on the

N^* decay amplitudes and the shift of the resonance position. Then the resonance mass M_R^J and the N^* decay amplitudes $\mathcal{M}_{N^* \rightarrow \gamma N, \omega N}$ can be identified with the quark model predictions of Refs. [5,6], as discussed in Refs. [24,27]. We however do not have information about the total decay width $\Gamma^J(s)$ for most of the N^* 's considered here. For simplicity, we assume that its energy-dependence is similar to the width of the $N^* \rightarrow \pi N$ decay within the oscillator constituent quark model. Following Ref. [27] and neglecting the real part of the mass shift, we then have

$$\Gamma^J(s) = \Gamma_0^J \frac{\rho(k_\pi)}{\rho(k_{0\pi})} \left(\frac{k_\pi}{k_{0\pi}} \right)^{2L_\pi} \exp [2(\mathbf{k}_{0\pi}^2 - \mathbf{k}_\pi^2)/\Lambda^2], \quad (19)$$

where L_π is the orbital angular momentum of the considered πN state and

$$\rho(k) = \frac{k E_N E_\pi}{E_N + E_\pi}. \quad (20)$$

In the above equations, $k_\pi (\equiv |\mathbf{k}_\pi|)$ is the pion momentum at energy \sqrt{s} while $k_{0\pi}$ is evaluated at $\sqrt{s} = M_R^J$. Our choice of the total average width Γ_0^J and cutoff parameter Λ for Eq. (19) will be specified in Sec. IV.

By setting the photon momentum in the z -direction, the $N^* \rightarrow \gamma N$ amplitudes in Eq. (18) can be calculated from the helicity amplitudes A_λ listed in Ref. [5] from

$$\mathcal{M}_{\gamma N \rightarrow N^*}(\mathbf{k}; m_i, \lambda_\gamma; J, M_J) = \sqrt{2k} A_{M_J} \delta_{M_J, \lambda_\gamma + m_i} f(\mathbf{k}, \mathbf{k}_0), \quad (21)$$

where \mathbf{k}_0 is the photon momentum at the resonance position, i.e. at $\sqrt{s} = M_R^J$, and the factor $f(\mathbf{k}, \mathbf{k}_0)$ was introduced to evaluate the amplitude in the region where the photon momentum is off the resonant momentum \mathbf{k}_0 . To be consistent with the form factor of the total decay width (19), we set $f(\mathbf{k}, \mathbf{k}_0) = \exp[(\mathbf{k}_0^2 - \mathbf{k}^2)/\Lambda^2]$.

The $N^* \rightarrow \omega N$ amplitude takes the following form [28]

$$\begin{aligned} \mathcal{M}_{N^* \rightarrow N' \omega}(\mathbf{q}; m_f, m_\omega; J, M_J) &= 2\pi \sqrt{\frac{2M_R^J}{M_N |\mathbf{q}_0|}} \sum_{L, m_L, S, m_S} \langle L m_L S m_S | J m_J \rangle \\ &\times \langle 1 m_\omega \frac{1}{2} m_f | S m_S \rangle Y_{L m_L}(\hat{q}) G(L, S) (|\mathbf{q}|/|\mathbf{q}_0|)^L f(\mathbf{q}, \mathbf{q}_0), \quad (22) \end{aligned}$$

where $G(L, S)$'s are listed in Refs. [6,28], and \mathbf{q}_0 is the ω meson momentum at $\sqrt{s} = M_R^J$. Here we also include the extrapolation factor $f(\mathbf{q}, \mathbf{q}_0) = \exp[(\mathbf{q}_0^2 - \mathbf{q}^2)/\Lambda^2]$ like that for the $N^* \rightarrow \gamma N$ vertex in Eq. (21).

In this study, we consider 12 positive parity and 10 negative parity nucleon resonances up to spin-9/2. The resonance masses M_R^J , the transition amplitudes A_{M_J} , and $G(L, S)$ needed to evaluate Eqs. (18)-(22) are taken from Refs. [5,6] and are listed in Tables I and II. Three of them were seen in the πN channel with four-star rating, five of them with two-star rating, and one of them with one-star rating. These N^* 's are indicated in the last column (PDG) of Tables I and II. Clearly the majority of the predicted N^* 's are "missing" so far. Here we should also mention that we are not able to account for the resonances with its predicted masses less than the ωN threshold, since their decay vertex functions with an off-shell momentum are not available in Refs. [5,6].

IV. RESULTS AND DISCUSSIONS

The model defined in Secs. II and III involves some free parameters which must be specified. The Pomeron exchange model parameters, as given explicitly in Sec. II, are taken from a global fit to the total cross sections of ω , ρ , and ϕ photoproduction at high energies and will not be adjusted in this study. The Pomeron exchange becomes weak at low energies, as shown by the dot-dashed curves in Fig. 2. We therefore will determine the parameters of the other amplitudes mainly by considering the data at low energies.

The pseudoscalar-meson exchange amplitude in Eq. (9) depends on the cutoff parameters $\Lambda_{\pi(\eta)}$ and $\Lambda_{\omega\gamma\pi(\eta)}$ of Eq. (10). The η exchange is very weak for any choice of its cutoff parameters. For definiteness, we choose $\Lambda_\eta = 1.0$ GeV and $\Lambda_{\omega\gamma\eta} = 0.9$ GeV as determined in a study [29] of ϕ photoproduction. At low energies, the π exchange completely dominates the cross sections at forward angles. Its cutoff parameters Λ_π and $\Lambda_{\omega\gamma\pi}$ thus can be fixed by fitting the forward cross section data. Our best fit is obtained by setting $\Lambda_\pi = 0.6$ GeV and $\Lambda_{\omega\gamma\pi} = 0.7$ GeV. These values are slightly different from those of Ref. [14]. The resulting contributions from the pseudoscalar-meson exchange are the dashed curves in Fig. 2.

The resonant amplitude defined by Eqs. (18)-(22) depends on the oscillator parameter Λ and the averaged total width Γ_0^J . We find that our results are rather insensitive to the cutoff Λ in the range $\Lambda = 0.5 \sim 1.0$ GeV. We take the value $\Lambda = 1$ GeV which is the value of the standard harmonic oscillator constituent quark model [1]. For the averaged total width Γ_0^J , we are guided by the widths listed by the Particle Data Group [23]. For the N^* 's which have been observed and listed in the last column (PDG) of Tables I and II, their widths are all very large in the range of about $200 \sim 400$ MeV [23,30]. The other N^* 's considered in our calculations are expected to have similar large widths. We therefore choose the average of the values listed by PDG and set $\Gamma_0^J = 300$ MeV for all N^* 's included in our calculation. The resulting N^* contributions are the dotted curves in Fig. 2.

With the pseudoscalar-meson exchange and resonant amplitudes fixed by the above procedure, the parameters for the direct and crossed nucleon amplitude [Eqs. (12)-(15)] are then adjusted to fit the data. Here we consider $g_{\omega NN} = 7 \sim 11$ and $\kappa_\omega = 0$ as determined in a study of πN scattering and $\gamma N \rightarrow \pi N$ reaction [24]. This range of ωNN coupling constant is very close to $g_{\omega NN} = 10.35$ determined [31] recently from fitting the nucleon-nucleon scattering data. Thus the only free parameter in the fit is the cutoff parameter Λ_N of the form factor in Eq. (15). It turns out that the contributions from the direct and crossed nucleon terms are backward peaked, and Λ_N can be fairly well determined by total cross sections at backward scattering angles. Our best fits are obtained from setting $\Lambda_N = 0.5$ GeV with $g_{\omega NN} = 10.35$ and $\kappa_\omega = 0$. The corresponding contributions from the direct and crossed nucleon terms are the dot-dot-dashed curves in Fig. 2.

Our full calculations including all amplitudes illustrated in Fig. 1 are the solid curves in Fig. 2. The data can be described to a very large extent in the considered energy region $E_\gamma \leq 5$ GeV. It is clear that the contributions due to the N^* excitations (dotted curves) and the direct and crossed nucleon terms (dot-dot-dashed curves) help bring the agreement with the data at large angles. The forward angle cross sections are mainly due to the interplay between the pseudoscalar-meson exchange (dashed curves) and the Pomeron exchange (dot-dashed curves). The main problem here is in reproducing the data at $E_\gamma = 1.23$ GeV. This perhaps indicates that the off-shell contributions from N^* 's below ωN threshold are important at

very low energies. These sub-threshold N^* 's cannot be calculated from the informations available so far within the model of Refs. [5,6] and are neglected in our calculations. The investigation of this possibility is however beyond the scope of this work. The quality of our fit is comparable to that of Zhao *et al.* [2].

It is important to note here that various cutoff parameters determined above also fix the high energy behavior of our predictions. Thus the accuracy of our model must be tested by examining whether we are able to describe the total cross sections from threshold to very high energies. Our prediction (solid curves) are compared with the available data in Fig. 3. We see that our model indeed can reproduce the data very well except in the region close to $W = 5$ GeV where the Pomeron exchange (dot-dashed curve) and the sum of the other amplitudes (dashed curve) are comparable. It is interesting to note here that if we increase the Pomeron exchange strength C_V of Eq. (6) by about 10%, the total cross section data can be much better described without too much changes in describing the low energy data. However, the Pomeron exchange parameters are constrained by a global fit to all of data for ρ , ω , and ϕ photoproduction, and therefore such a change is not desirable. Instead, we must explore other mechanisms, such as the absorption effects due to the intermediate $N\rho$ state as discussed in Ref. [10]. Since the N^* excitations considered here are in the region $W \leq 2.5$ GeV, we need not to resolve the problem in this transition region near $W = 5$ GeV.

To have a better understanding of the resonance contributions, we compare in Fig. 4 the contributions from the considered N^* 's to the differential cross sections at $\theta = 90^\circ$. Here the N^* states listed in Tables I and II can be identified by its mass M_R^J . As also indicated in Fig. 4, the contributions from $N_{\frac{3}{2}}^{3+}(1910)$ and $N_{\frac{3}{2}}^{3-}(1960)$ are the largest at all energies. From Tables I and II, we see that the $N_{\frac{3}{2}}^{3+}(1910)$ is a missing resonance, while $N_{\frac{3}{2}}^{3-}(1960)$ is identified by Capstick [32] as a two star resonance $D_{13}(2080)$ of PDG. In the study of Zhao et al. [2,3], they found that $F_{15}(2000)$ dominates. This resonance is identified with $N_{\frac{5}{2}}^{5+}(1995)$ in Table I and is found to be not so strong in our calculation, as also indicated in Fig. 4. This significant difference between the two calculations is not surprising since the employed quark models are rather different. In particular, our predictions include the configuration mixing effects due to residual quark-quark interactions.

In Fig. 4 we also see that the relative importance between different resonances depend on the photon energy. As expected from the resonance part expression (18), the higher mass resonances become more important as the photon energy increases from 1.23 GeV ($W = 1.79$ GeV) to 1.92 GeV ($W = 2.11$ GeV). For example, we also indicate in Fig. 4 that the contribution from $N_{\frac{7}{2}}^{7-}(2090)$, identified in Table II with $G_{17}(2190)$ of PDG, becomes comparable to that of $N_{\frac{3}{2}}^{3+}(1910)$ at $W = 2.11$ GeV.

The total resonance effects are shown in Fig. 5. The solid curves are from our full calculations, while the dotted curves are from the calculations without including N^* excitations. The results shown in Fig. 5 indicate that it is rather difficult to test our predictions by considering only the angular distributions, since the N^* 's influence is mainly in the large scattering angle region where accurate measurements are perhaps still difficult. On the other hand, the forward cross sections seem to be dominated by the well-understood pseudoscalar-meson exchange (less-understood η exchange is negligibly small here) and Pomeron exchange. Therefore, one can use this well-controlled background to examine the N^* contributions by exploiting the interference effects in the spin observables.

We first examine the spin observables discussed in Refs. [2,3]. Our predictions for photon asymmetry (Σ_x), target asymmetry (T_y), recoil nucleon asymmetry (P_y), and tensor polarization ($V_{z'z'}$) are shown in Fig. 6. These single polarization observables are calculated according to the definitions given, e.g., in Refs. [26,35]. We see that the N^* excitations can change the predictions from the dotted curves to solid curves. The dashed curves are obtained when only the $N_{\frac{3}{2}}^{3+}(1910)$ and $N_{\frac{3}{2}}^{3-}(1960)$ are included in calculating the resonant part of the amplitude. Our predictions are significantly different from those of Refs. [2,3]. As mentioned above, this is perhaps mainly due to the differences between the employed quark models. Nevertheless, we confirm their conclusion that the single polarization observables are sensitive to the N^* excitations but mostly at large scattering angles. The vector asymmetry V_y has also been investigated, but is not presented here since it is almost impossible to access experimentally [36].

To further facilitate the experimental tests of our predictions, we have also investigated other spin observables. We have identified two polarization observables which are sensitive to the N^* contributions at forward angles, where precise measurements might be more favorable because the cross sections are peaked at $\theta = 0$ (see Fig. 2). The first one is the parity asymmetry defined as [37]

$$P_\sigma = \frac{d\sigma^N - d\sigma^U}{d\sigma^N + d\sigma^U} = 2\rho_{1-1}^1 - \rho_{00}^1, \quad (23)$$

where σ^N and σ^U are the cross sections due to the natural and unnatural parity exchanges respectively, and $\rho_{\lambda,\lambda'}^i$ are the vector-meson spin density matrices. For the dominant one-pion exchange amplitude, which has unnatural parity exchange only, one expects $P_\sigma = -1$. Thus any deviation from this value will be only due to N^* excitation and Pomeron exchange, since the contribution from the direct and crossed nucleon terms is two or three orders in magnitude smaller at $\theta = 0$ (see Fig. 2). Our predictions for P_σ are shown in Fig. 7. We show the results from calculations with (solid curve) and without (dotted curve) including N^* contributions. The difference between them is striking and can be unambiguously tested experimentally. In the considered low energy region, most of the N^* excitations involve both the natural and unnatural parity exchanges. The rapid energy-dependence of the solid curve thus reflects the change of relative importance between different N^* 's as energy increases, as seen in Fig. 4. At $W \geq 2.5$ GeV, the Pomeron exchange starts to dominate and shift the prediction to the $P_\sigma = +1$ limit of natural parity exchange. Here we also find that the $N_{\frac{3}{2}}^{3+}(1910)$ and $N_{\frac{3}{2}}^{3-}(1960)$ are dominant. By keeping only these two resonances in calculating the resonant part of the amplitude, we obtain dashed curve which is not too different from the full calculation (solid curve).

We also find that the beam-target double asymmetry at forward angles is sensitive to the N^* excitations. It is defined as [26]

$$C_{zz}^{BT} = \frac{d\sigma(\uparrow\downarrow) - d\sigma(\uparrow\uparrow)}{d\sigma(\uparrow\downarrow) + d\sigma(\uparrow\uparrow)}, \quad (24)$$

where the arrows represent the helicities of the incoming photon and the target protons. In Fig. 8, we present our predictions on C_{zz}^{BT} at $\theta = 0$ as a function of invariant mass W . The striking difference between the solid curve and dotted curve is due to the N^* excitations. At

$W \geq 2.5$ GeV this asymmetry vanishes since all amplitudes except the helicity-conserving natural parity Pomeron exchange are suppressed at high energies. The role of N^* here is similar to what is discussed above for P_σ . Again, the $N_{\frac{3}{2}}^+(1910)$ and $N_{\frac{3}{2}}^-(1960)$ give the dominant contributions. This is evident from comparing the solid curve and the dashed curve which is obtained when only these two resonances are kept in calculating the resonant part of the amplitude. It is very interesting to note that the $N_{\frac{3}{2}}^-(1960)$ is also found to be important in kaon photoproduction [38], although its identification with the $D_{13}(2080)$ is still controversial. Our predictions show that ω photoproduction can be useful in resolving this issue.

V. FUTURE DEVELOPMENTS

In this work, we have investigated the role of nucleon resonances in ω photoproduction. The resonance parameters are taken from the predictions of Refs. [5,6]. It is found that the resonant contributions can influence significantly the differential cross sections at large angles. We have presented predictions showing the N^* effects on several spin observables. In particular, we have shown that our predictions can be crucially tested by measuring the parity asymmetry and beam-target double asymmetry at $\theta = 0$. The dominant contributions are found to be from $N_{\frac{3}{2}}^+(1910)$, a missing resonance, and $N_{\frac{3}{2}}^-(1960)$ which was indentified [5] as the two star resonance $D_{13}(2080)$ of PDG. Experimental test of our predictions will be a useful step toward resolving the so-called “missing resonance problem” or distinguishing different quark model predictions.

To end, we should emphasize that the present investigation is a very first step from the point of view of a dynamical treatment of the problem, as has been done for the πN scattering and pion photoproduction [24,27]. The main uncertain part is the lack of a complete calculation of the $N^* \rightarrow \gamma N, \omega N$ transition form factors given in Eqs. (21) and (22). The use of the extrapolation factor $f(\mathbf{k}, \mathbf{k}_0) = \exp[(\mathbf{k}_0^2 - \mathbf{k}^2)/\Lambda^2]$ must be justified by extending the calculations of Refs. [5,6] to evaluate these form factors for any off-shell momentum. It is also needed to generate the form factors for the N^* 's which are below ωN threshold and are neglected in this investigation. The effects due to the sub-threshold N^* 's could be important in explaining the data very close to ωN threshold [e.g., Fig. 2(a) at $E_\gamma = 1.23$ GeV]. An another necessary step is to develop an approach to calculate the crossed N^* amplitude [similar to the crossed nucleon amplitude Fig. 1(d)] using the same relativised constituent quark model employed in Refs. [5,6]. Finally, the effects due to the initial and final state interactions must be also investigated, which may be pursued by extending the approach of Ref. [10].

ACKNOWLEDGMENTS

This work was supported in part by National Science Council of Republic of China, Russian Foundation for Basic Research under Grant No. 96-15-96426, and U.S. DOE Nuclear Physics Division Contract No. W-31-109-ENG-38.

REFERENCES

- [1] N. Isgur and G. Karl, Phys. Lett. **72B**, 109 (1977); Phys. Rev. D **18**, 4187 (1978); **19**, 2653 (1979), **23**, 817(E) (1981); R. Koniuk and N. Isgur, *ibid.* **21**, 1868 (1980).
- [2] Q. Zhao, Z. Li, and C. Bennhold, Phys. Lett. B **436**, 42 (1998); Phys. Rev. C **58**, 2393 (1998).
- [3] Q. Zhao, Talk at 8th International Conference on Hadron Spectroscopy, Beijing, China, Aug. 1999, nucl-th/9909060.
- [4] Q. Zhao, J.-P. Didelez, M. Guidal, and B. Saghai, Nucl. Phys. **A660**, 323 (1999).
- [5] S. Capstick, Phys. Rev. D **46**, 2864 (1992).
- [6] S. Capstick and W. Roberts, Phys. Rev. D **49**, 4570 (1994).
- [7] S. Godfrey and N. Isgur, Phys. Rev. D **32**, 189 (1985); S. Capstick and N. Isgur, *ibid.* **34**, 2809 (1986).
- [8] See, for example, A. Le Yaouanc, L. Oliver, O. Pene, and J. C. Raynal, *Hadron Transitions in the Quark Model* (Gordon and Breach, New York, 1988).
- [9] Aachen-Berlin-Bonn-Hamburg-Heidelberg-Munich Collaboration, R. Erbe *et al.*, Phys. Rev. **175**, 1669 (1968)
- [10] K. Schilling and F. Storim, Nucl. Phys. **B7**, 559 (1968).
- [11] H. Fraas, Nucl. Phys. **B36**, 191 (1972).
- [12] J. Ballam *et al.*, Phys. Rev. D **7**, 3150 (1973);
- [13] P. Joos *et al.*, Nucl. Phys. **B122**, 365 (1977).
- [14] B. Friman and M. Soyeur, Nucl. Phys. **A600**, 477 (1996).
- [15] J. D. Bjorkin and S. D. Drell, *Relativistic Quantum Fields* (McGraw-Hill, 1964).
- [16] A. Donnachie and P. V. Landshoff, Nucl. Phys. **B244**, 322 (1984); **B267**, 690 (1986); Phys. Lett. B **185**, 403 (1987); **296**, 227 (1992).
- [17] J.-M. Laget and R. Mendez-Galain, Nucl. Phys. **A581**, 397 (1995).
- [18] M. A. Pichowsky and T.-S. H. Lee, Phys. Rev. D **56**, 1644 (1997).
- [19] J.-R. Cudell, K. Kang, and S. K. Kim, Phys. Lett. B **395**, 311 (1997).
- [20] L. Tiator, C. Bennhold, and S. S. Kamalov, Nucl. Phys. **A580**, 455 (1994).
- [21] J. J. de Swart, Rev. Mod. Phys. **35**, 916 (1963).
- [22] F. E. Close and R. G. Roberts, Phys. Lett. B **316**, 165 (1993).
- [23] Particle Data Group, C. Caso, *et al.*, Eur. Phys. J. C **3**, 1 (1998).
- [24] T. Sato and T.-S. H. Lee, Phys. Rev. C **54**, 2660 (1996).
- [25] H. Haberzettl, C. Bennhold, T. Mart, and T. Feuster, Phys. Rev. C **58**, 40 (1998).
- [26] A. I. Titov, Y. Oh, S. N. Yang, and T. Morii, Phys. Rev. C **58**, 2429 (1998).
- [27] T. Yoshimoto, T. Sato, M. Arima, and T.-S. H. Lee, Phys. Rev. C **61**, 065203 (2000).
- [28] S. Capstick, private communications.
- [29] A. I. Titov, T.-S. H. Lee, H. Toki, and O. Streltsova, Phys. Rev. C **60**, 035205 (1999).
- [30] D. M. Manley and E. M. Saleski, Phys. Rev. D **45**, 4002 (1992).
- [31] Th. A. Rijken, V. G. J. Stoks, and Y. Yamamoto, Phys. Rev. C **59**, 21 (1999).
- [32] S. Capstick, Phys. Rev. D **46**, 1965 (1992).
- [33] F. J. Klein, Ph.D. thesis, Bonn Univ. (1996); SAPHIR Collaboration, F. J. Klein *et al.*, π N Newsllett. **14**, 141 (1998).
- [34] J. Ballam *et al.*, Phys. Lett. **30B**, 421 (1969); AHHM Collaboration, W. Struczinski *et*

- al.*, Nucl. Phys. **B108**, 45 (1976); D. P. Barber *et al.*, Z. Phys. C **26**, 343 (1984); ZEUS Collaboration, M. Derrick *et al.*, *ibid.* **73**, 73 (1996).
- [35] M. Pichowsky, Ç. Şavkli, and F. Tabakin, Phys. Rev. C **53**, 593 (1996).
- [36] W. M. Kloet, W.-T. Chiang, and F. Tabakin, Phys. Rev. C **58**, 1086 (1998).
- [37] K. Schilling, P. Seyboth, and G. Wolf, Nucl. Phys. **B15**, 397 (1970).
- [38] T. Mart and C. Bennhold, Phys. Rev. C **61**, 012201 (1999).

TABLES

N^*	M_R^J	$A_{1/2}$	$A_{3/2}$	$G(1, 1/2)$	$G(1, 3/2)$		$\sqrt{\Gamma_{N\omega}^{\text{tot}}}$	PDG [23]
$N_{\frac{1}{2}}^{1+}$	1880	0	—	-4.3	-1.6	—	4.6	
$N_{\frac{1}{2}}^{1+}$	1975	-12	—	-3.1	-0.8	—	3.1	
				$G(1, 1/2)$	$G(1, 3/2)$	$G(3, 3/2)$		
$N_{\frac{3}{2}}^{3+}$	1870	-2	-15	0.0	+4.4	+0.6	4.5	$F_{13}(1900)^{**}$
$N_{\frac{3}{2}}^{3+}$	1910	-21	-27	-5.8	+5.7	-0.5	8.2	
$N_{\frac{3}{2}}^{3+}$	1950	-5	2	-5.4	-3.2	+0.7	6.3	
$N_{\frac{3}{2}}^{3+}$	2030	-9	15	-1.6	-2.9	+0.7	3.3	
				$G(3, 1/2)$	$G(1, 3/2)$	$G(3, 3/2)$		
$N_{\frac{5}{2}}^{5+}$	1980	-11	-6	+2.1	-1.7	-1.1	2.9	
$N_{\frac{5}{2}}^{5+}$	1995	-18	1	-0.3	+3.1	-1.6	3.5	$F_{15}(2000)^{**}$
				$G(3, 1/2)$	$G(3, 3/2)$	$G(5, 3/2)$		
$N_{\frac{7}{2}}^{7+}$	1980	-1	-2	-0.8	+1.4	0.0	1.6	$F_{17}(1990)^{**}$
$N_{\frac{7}{2}}^{7+}$	2390	-14	-11	-0.8	+2.1	+2.0	3.0	
$N_{\frac{7}{2}}^{7+}$	2410	+1	-1	-0.7	+1.3	0.0	1.5	
				$G(5, 1/2)$	$G(3, 3/2)$	$G(5, 3/2)$		
$N_{\frac{9}{2}}^{9+}$	2345	-29	+13	-0.3	-2.9	-0.6	2.9	$H_{19}(2220)^{****}$

TABLE I. Parameters for positive parity nucleon resonances from Refs. [5,6]. The helicity amplitude A_λ is given in unit of $10^{-3} \text{ GeV}^{-1/2}$. $G(L, S)$ and $\sqrt{\Gamma_{N\omega}^{\text{tot}}}$ are in unit of $\text{MeV}^{1/2}$. The resonance mass M_R^J is in unit of MeV.

N^*	M_R^J	$A_{1/2}$	$A_{3/2}$	$G(0, 1/2)$	$G(2, 3/2)$		$\sqrt{\Gamma_{N\omega}^{\text{tot}}}$	PDG [23]
$N_{\frac{1}{2}}^{1-}$	1945	+12	—	-0.9	-5.6		5.7	$S_{11}(2090)^*$
$N_{\frac{1}{2}}^{1-}$	2030	+20	—	-0.1	-2.8		2.8	
				$G(2, 1/2)$	$G(0, 3/2)$	$G(2, 3/2)$		
$N_{\frac{3}{2}}^{3-}$	1960	+36	-43	-4.3	-0.2	-4.6	6.3	$D_{13}(2080)^{**}$
$N_{\frac{3}{2}}^{3-}$	2055	+16	0	+2.0	-1.3	-2.7	3.6	
$N_{\frac{3}{2}}^{3-}$	2095	-9	-14	-3.2	+1.9	+3.8	5.3	
				$G(2, 1/2)$	$G(2, 3/2)$	$G(4, 3/2)$		
$N_{\frac{5}{2}}^{5-}$	2080	-3	-14	-2.2	-0.3	+2.0	2.9	
$N_{\frac{5}{2}}^{5-}$	2095	-2	-6	-3.1	+3.3	+0.8	4.6	$D_{15}(2200)^{**}$
				$G(4, 1/2)$	$G(2, 3/2)$	$G(4, 3/2)$		
$N_{\frac{7}{2}}^{7-}$	2090	-34	+28	-1.5	-3.7	-1.7	4.4	$G_{17}(2190)^{****}$
$N_{\frac{7}{2}}^{7-}$	2205	-16	+4	-0.2	-5.1	+0.3	5.1	
				$G(4, 1/2)$	$G(4, 3/2)$	$G(6, 3/2)$		
$N_{\frac{9}{2}}^{9-}$	2215	0	+1	-1.0	+1.7	0.0	2.0	$G_{19}(2250)^{****}$

TABLE II. Parameters for negative parity nucleon resonances from Refs. [5,6]. The units are the same as in Table I.

FIGURES

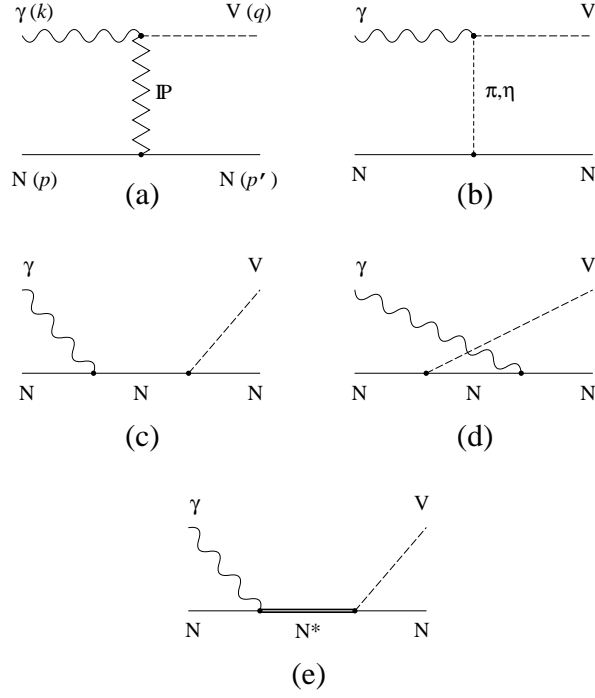


FIG. 1. Diagrammatic representation of ω photoproduction mechanisms: (a) Pomeron exchange, (b) (π, η) exchange, (c) direct nucleon term, (d) crossed nucleon term, and (e) s -channel nucleon excitations.

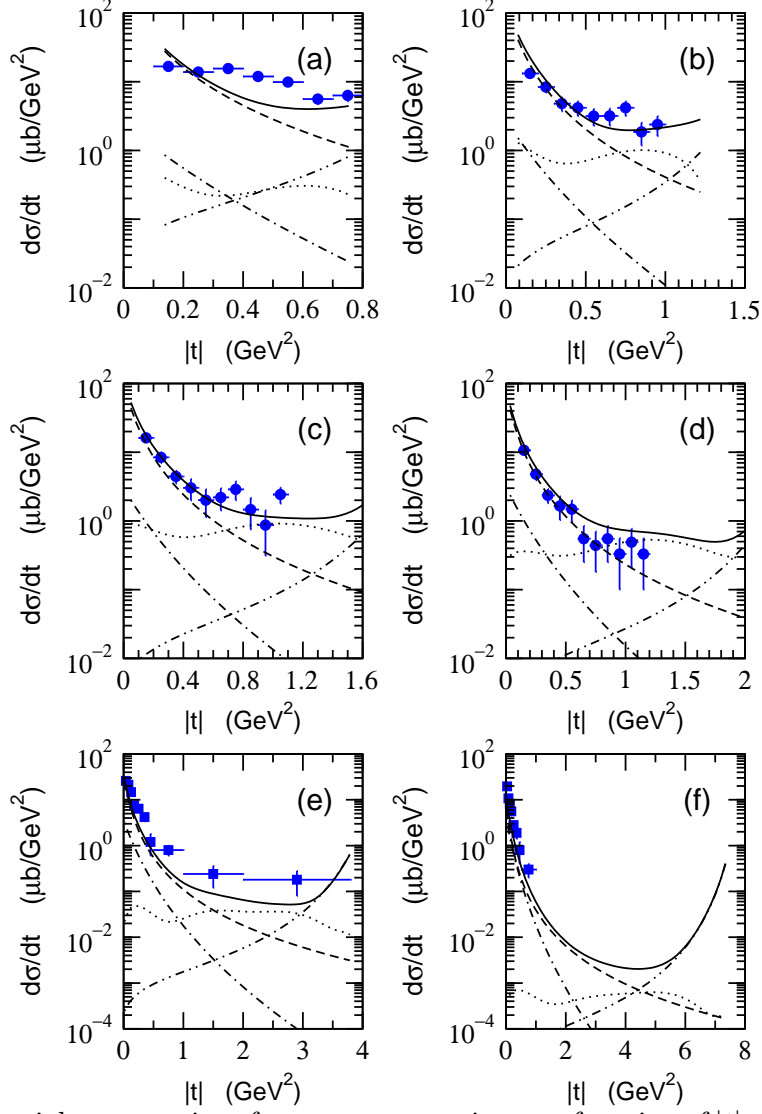


FIG. 2. Differential cross sections for $\gamma p \rightarrow p\omega$ reaction as a function of $|t|$ at $E_\gamma =$ (a) 1.23, (b) 1.45, (c) 1.68, (d) 1.92, (e) 2.8, and (f) 4.7 GeV. The results are from pseudoscalar-meson exchange (dashed), Pomeron exchange (dot-dashed), direct and crossed nucleon terms (dot-dot-dashed), N^* excitation (dotted), and the full amplitude (solid). Data are taken from Ref. [33] (filled circles) and Ref. [12] (filled squares).

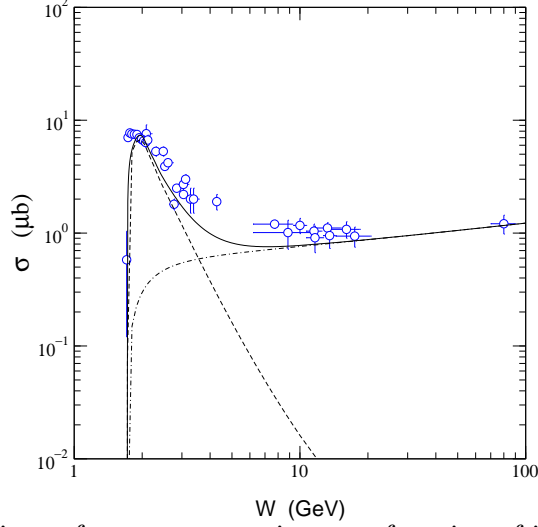


FIG. 3. Total cross sections of $\gamma p \rightarrow p\omega$ reaction as a function of invariant mass W . The solid curve is from the full calculation and the dotted curve is from the calculation without including Pomeron exchange. The Pomeron exchange contribution is given by the dot-dashed line. Data are taken from Refs. [12,33,34].

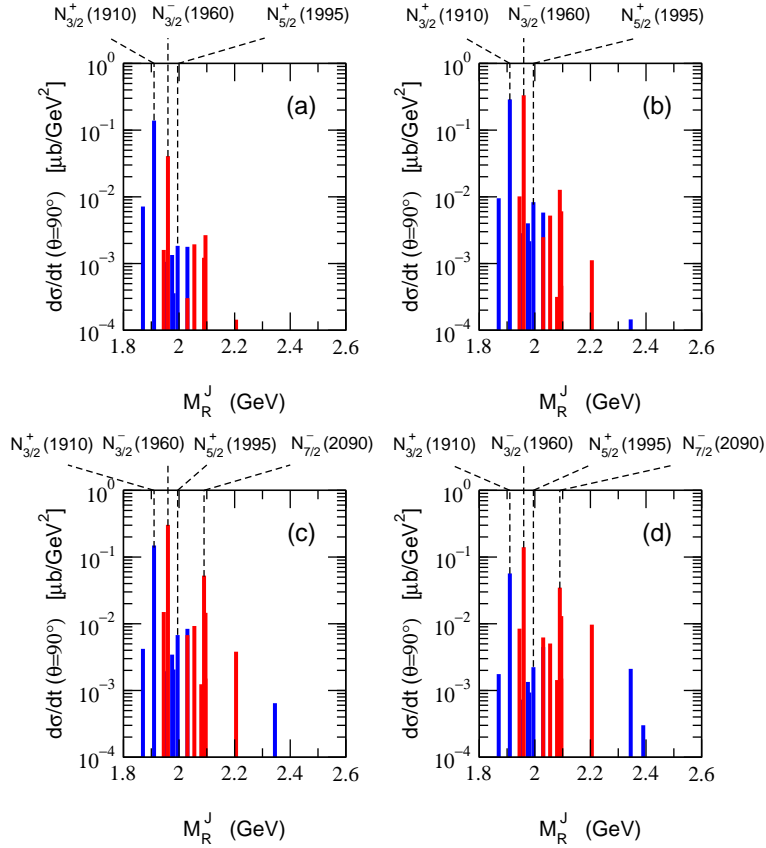


FIG. 4. Contribution from each N^* listed in Tables I and II to the differential cross sections at $\theta = 90^\circ$ and $E_\gamma =$ (a) 1.23, (b) 1.45, (c) 1.68, and (d) 1.92 GeV, which corresponds to $W =$ (a) 1.79, (b) 1.90, (c) 2.01, and (d) 2.11 GeV, respectively.

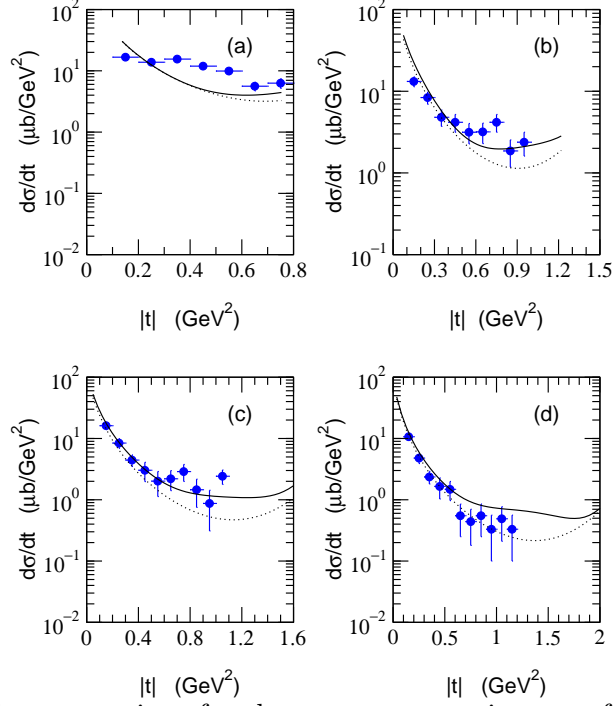


FIG. 5. Differential cross sections for the $\gamma p \rightarrow p\omega$ reaction as a function of $|t|$ at different energies: $E_\gamma =$ (a) 1.23, (b) 1.45, (c) 1.68, and (d) 1.92 GeV. The solid and dotted curves are calculated respectively with and without including N^* effects. Data are taken from Ref. [33].

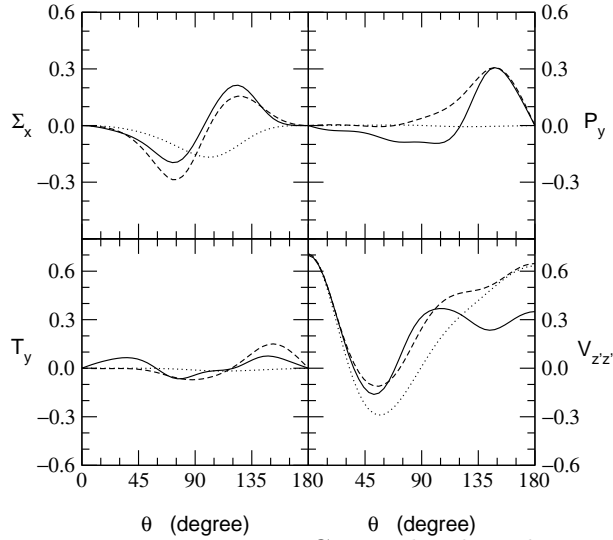


FIG. 6. Single asymmetries at $E_\gamma = 1.7$ GeV. The dotted curves are calculated without including N^* effects, the dashed curves include contributions of $N_{\frac{3}{2}}^{3+}(1910)$ and $N_{\frac{3}{2}}^{3-}(1960)$ only, and the solid curves are calculated with all N^* 's listed in Tables I and II.

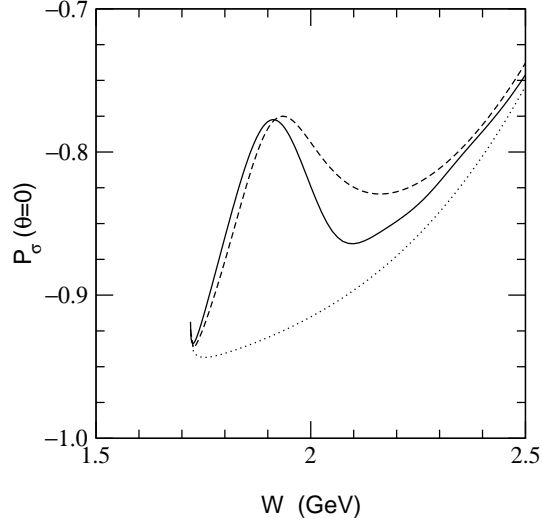


FIG. 7. Parity asymmetry P_σ at $\theta = 0$ as a function of W . Notations are the same as in Fig. 6.

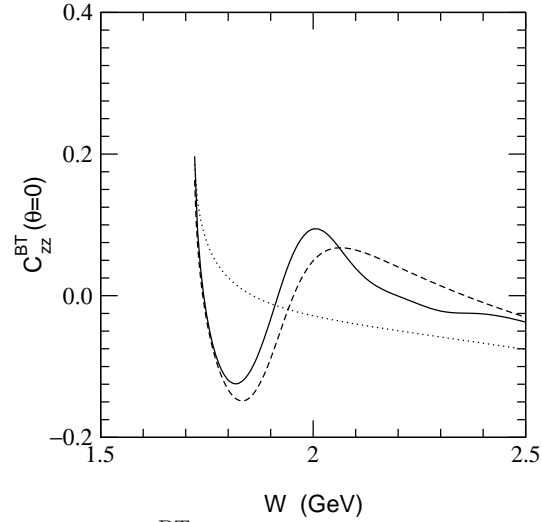


FIG. 8. Beam-target asymmetry C_{zz}^{BT} at $\theta = 0$ as a function of W . Notations are the same as in Fig. 6.